# Metal-Free Growth of Nanographene on Silicon Oxides for Transparent Conducting Applications

*Henry Medina, Yung-Chang Lin, Chuanhong Jin, Chun-Chieh Lu, Chao-Hui Yeh, Kun-Ping Huang, Kazu Suenaga, John Robertson, and Po-Wen Chiu**

**Conventional methods to prepare large-area graphene for transparent conducting electrodes involve the wet etching of the metal catalyst and the transfer of the graphene film, which can degrade the film through the creation of wrinkles, cracks, or tears. The resulting films may also be obscured by residual metal impurities and polymer contaminants. Here, it is shown that direct growth of large-area flat nanographene films on silica can be achieved at low temperature (400 °C) by chemical vapor deposition without the use of metal catalysts. Raman spectroscopy and TEM confirm the formation of a hexagonal atomic network of $sp^2$-bonded carbon with a domain size of about 3–5 nm. Further spectroscopic analysis reveals the formation of SiC between the nanographene and $SiO_2$, indicating that SiC acts as a catalyst. The optical transmittance of the graphene films is comparable with transferred CVD graphene grown on Cu foils. Despite the fact that the electrical conductivity is an order of magnitude lower than CVD graphene grown on metals, the sheet resistance remains 1–2 orders of magnitude better than well-reduced graphene oxides.**

## 1. Introduction

Graphene is a single atomic layer of $sp^2$ carbon on a honeycomb lattice. It is transparent, flexible, and highly conductive due to its dispersionless band structure near the Fermi level.[1] At room temperature, charge carriers can travel without scattering over hundreds of nanometers,[2] resulting in a very high mobility. The optical transparency of a single layer can be as high as 97%.[3] Graphene is also chemically inert and can be synthesized on a large scale without the need for sophisticated production techniques.[4,5] These remarkable properties have fueled intensive research on graphene aiming to replace tin-doped indium oxide (ITO), the current commercially dominant transparent conducting oxide. Although the conductivity of large-scale graphene sheets must be improved to rival that of ITO, graphene's high optical transparency and flexibility, along with its unlimited scalability, provide a strong incentive to explore its use in future optoelectronic devices. To develop graphene-based electrodes, however, some hurdles must be overcome, specifically the development of a method for the direct growth of graphene on insulating substrates without any transfer or etch-off process.

Transition metals such as Fe, Cu, and Ni have long been regarded as key ingredients for growing $sp^2$ carbon nanostructures due to their superior catalytic dissociation of carbon-containing molecules and graphitization of carbon atoms. New studies have made use of Ni-Au as a catalyst for graphene grown at low temperature[6]; however, the electrical properties are yet to be tested. Recently, chemical vapor deposition (CVD) growth of carbon nanotubes using semiconductor or oxide nanoparticles as a catalyst has become possible.[7–9] These surprising findings show that the growth requires nanoparticle catalysts which are not limited in composition to the commonly employed transition metals. The results also imply that direct deposition of graphene on oxides is possible, even if the growth mechanism may be different due to the higher dimensionality. Rummeli et al. showed in their electron microscopic studies that nanographene flakes can be formed on MgO without using metal catalysts.[10] Later on, other insulating substrates such as SiN, Si, $Al_2O_3$, and $SiO_2$ were also proposed as potential catalysts for graphitization.[11–14] It was speculated that graphene-like films would form on these substrates according to their Raman spectra. The common features of these Raman spectra are the fairly low 2D over G intensity ratios and the overlap of broadened G and D modes, indicative of the poor crystalline quality and of the massive coexisting amorphous carbons. Moreover, no electron microscopic identifications and transport characterizations were provided in these reports to support the argument of graphene formation on the

H. Medina, Y.-C. Lin, C.-C. Lu, C.-H. Yeh, Prof. P.-W. Chiu
Department of Electrical Engineering
National Tsing Hua University
Hsinchu 30013, Taiwan
E-mail: pwchiu@ee.nthu.edu.tw
Dr. C. Jin, Dr. K. Suenaga
National Institute of Advanced Industrial Science and Technology (AIST)
Tsukuba 305-8565, Japan
Dr. K.-P. Huang
Mechanical and Systems Research Laboratories
Industrial Technology Research Institute Hsinchu 31040, Taiwan
Prof. J. Robertson, Prof. P.-W. Chiu
Cambridge University
Engineering Department
9 JJ Thomson Avenue
Cambridge CB3 0FA, UK

**DOI: 10.1002/adfm.201102423**

insulating substrates. In this article, we show that continuous nanographene films can be directly grown on silicon oxides at a temperature greater than 400 °C using electron cyclotron resonance CVD (ECR-CVD). The sp*2* nature and the crystalline quality of the resulting films were examined by Raman spectroscopy and transmission electron microscopy (TEM). At room temperature, the films showed ohmic behavior and ambipolar transport characteristics in the gate sweeps. The transfer-free process results in highly reproducible fabrication and opens up a facile route for its direct applications in optoelectronic devices such as transparent conducting films that do not require conductivity as high as ITO.

## 2. Results and Discussion

Direct ECR-CVD deposition of nanographene begins by surface cleaning with a mixture of argon and hydrogen plasma for several minutes, thus removing most of the organic contaminants from the surface. In the growth, $C_2H_4$ plasma, along with Ar to stabilize the plasma, is ignited in a very low gas flow rate (0.12 sccm). A thin nanographene film can be formed on the oxide surface at a temperature higher than 400 °C. The distance between the sample and plasma is found to be crucial to the quality of the resulting films, which is also varied with the plasma power applied. Mild post annealing under a hydrogen atmosphere is used to remove excess amorphous carbons on top and to enhance the conductivity of the films. **Figure 1**a,b shows the optical photographs of ECR-CVD nanographene films grown on quartz substrates. The film thickness is controlled by the deposition time. Direct deposition of nanographene on curved surfaces is also possible (Figure 1b). However, inhomogeneous film thickness may exist due to the temperature gradient on the substrates. Figure 1c shows a scanning electron microscopy (SEM) image of the nanographene film grown on quartz for a long time with a scratch made after the growth. The scratched area accumulates charges on bare quartz surface during the SEM observation and causes a sharp contrast with the area covered by nanographene layers, showing the conductive behavior and the uniformity of the film.

To obtain the crystalline structure, we transfer the films onto TEM grids (Mo quantifoils) using a technique reported previously.[15] The film is found to be flat and continuous, without wrinkles or humps over the transferred area on the grid, as can be seen piecewise in **Figure 2**a. We also notice that low-density nanopores exist, with diameters ranging from 1 to 10 nm.

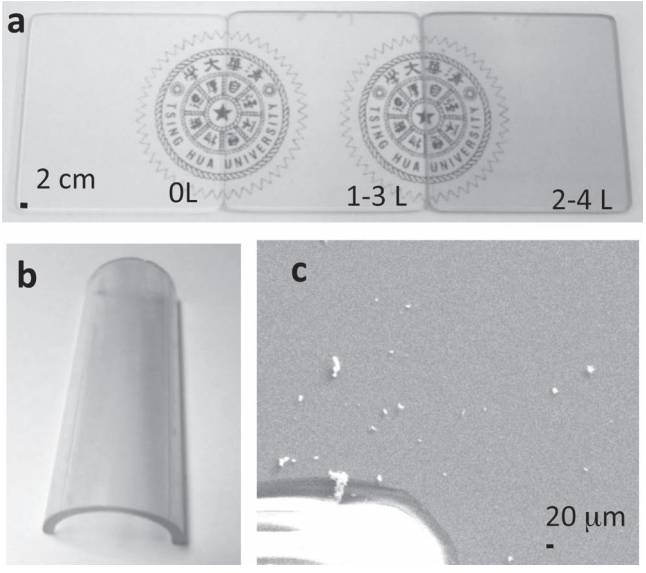


**Figure 1.** Direct deposition of ECR-CVD nanographene on quartz. a) Nanographene films with different thicknesses obtained by varying the growth time. b) Nanographene deposition on a 1 in. half cylinder. c) SEM image of nanographene on a quartz plate. The bright area corresponds to the bare substrate made by a scratch. The quartz particles and the scratched area give a good contrast to the area with nanographene film.

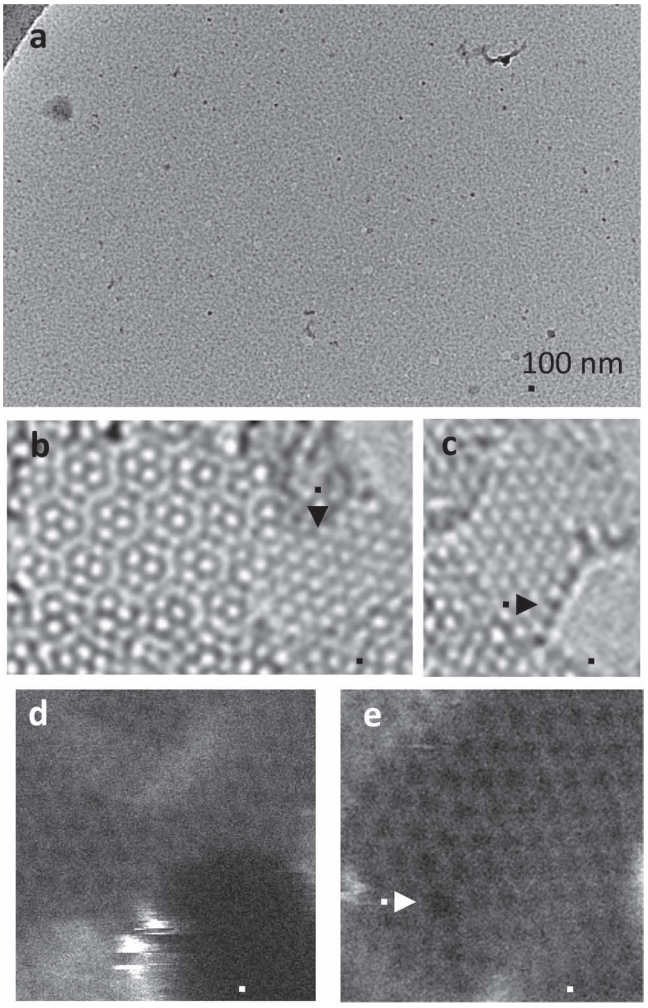


**Figure 2.** TEM images of ECR-CVD nanographene films grown on $SiO_2$. a) Low-magnification image, showing a flat and continuous free-standing nanographene film piecewise. b) A zoom-in image with an arrow pointing to the single-layer region. c) A zoom-in image with an arrow pointing to the Si atoms terminated at the edge of the single-layer region. d,e) Scanning transmission electron microscopy images of graphene showing the edge termination of a single-layer nanographene and a point defect inside a single-layer domain, respectively. Scale bars are 3 Å in (b) and (c), 5 Å in (d) and (e).

These nanopores are intrinsic structural defects and distributed randomly in the film. It is known that focused high-energy electron beam irradiation also generates similar nanopores during observations; therefore a low acceleration voltage (60 kV) was used to avoid irradiation-induced damages.[16]

Figure 2b,c shows typical atomic-resolution TEM images of ECR-CVD nanographene. The film is made up of single, double, and few-layer nanographene, with turbostratic stacking orders. The thickness is non-uniform over the entire film. For the samples with highest optical transmittance (approximately 94%), it consists mainly of 1–3 layers. The single-layer regions can be observed from place to place in the films, as exemplified in Figure 2b,c, and account for 20% of the area in typical ECR-CVD nanographene. The domain size of nanographene ranges from 3 to 5 nm, depending on the growth rate and temperature. A few regions containing topological defects appear inside the domains as well as on the bridges between nanopores. Figures 2d,e shows scanning transmission electron microscopy images for the edge termination and point defects inside a single-layer domain, respectively. The film quality (in terms of domain size and defect density) for nanographene grown on quartz is found to be quite similar to that on $SiO_2$.

CVD growth of graphene begins with catalyst-assisted hydrocarbon dissociation, followed by diffusion and graphitization of carbon atoms on the catalyst surface. Transition metals such as Cu, Ni, and Ru are commonly employed as catalysts for the growth.[4,17] Of particular interest here is the use of silicon oxide as a catalyst. A key question then is whether silicon oxide alone functions as the graphitization catalyst. To provide more insight into the underlying mechanism, we studied the evolution of Raman spectra with growth time and before the first nanographene layers are formed (**Figure 3**a). A broad and asymmetric peak between 670 and 900 $cm^{-1}$ is seen in early stages of graphene growth, indicating that SiC forms before graphitization takes place. The SiC characteristic peaks are still visible after complete nanographene coverage formed on the substrate. The presence of SiC is also confirmed by X-ray photoelectron spectroscopy (XPS) in Figure 3b. In early stages of growth, the *C*1s spectra can be explicitly deconvoluted into two components. The primary peak appears at 283.8 eV and progressively shifts to higher binding energy as growth time increases. It eventually moves to 284.4 eV, identifying the formation of an $sp^2$ C–C network of the grown film. A weak shoulder shows up at 282.3 eV in early stages of growth, which is the fingerprint of Si–C bonds formed in the plasma-enhanced CVD process.[18] It is known that SiC can be formed through solid-state carbon reduction of silica, but only at significantly higher temperatures. In the typical CVD growth of graphene (at 800–1000 °C) without plasma, no carbide forms on flat $SiO_2$ substrates and, hence, no graphene grows without metal catalysts. Also of note is that $sp^2$ carbon on SiC is not usually observed in the typical carbothermal process. It is thereore plausible to attribute the formation of SiC to the reduction reactions driven by the energetic hydrocarbon radicals. To confirm this argument, we performed a control experiment in which plasma was not ignited in the CVD process, finding that neither SiC nor graphene was formed on flat $SiO_2$ substrates. The SiC buffer layer can be formed through the reaction:[19] $3C + SiO_2 \rightarrow SiC + 2CO$.

The carbothermal reduction of silica presents the rate-limiting step in the growth of nanographene on $SiO_2$. Under the growth conditions described above, it takes around 4 min to form the SiC layer. Once this SiC layer is formed, only about 1 min is required for complete nanographene coverage. The SiC layer acts as a catalyst to dissociate the hydrocarbon gas, but it is self-limiting process and only few nanographene layers form. Hydrocarbon molecules only dissociate on the SiC, not on the nanographene layer itself. Carbon atoms formed on the SiC layer add to the edges of nanographene nuclei, thus growing the domains, without surface mobility of the C on SiC. The small domain size of the nanographene implies poor surface mobility of the C on SiC.

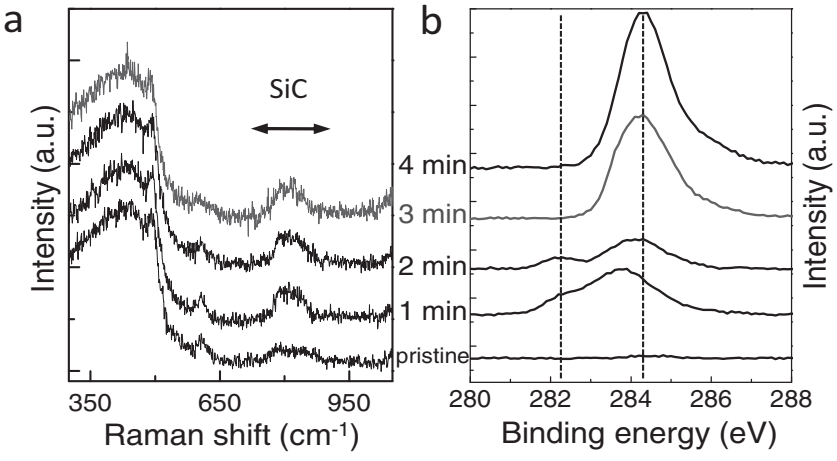


**Figure 3.** Evidence of SiC formation on quartz substrates in the ECR-CVD growth of nanographene. a) Raman spectra taken by 514 nm laser excitation show the characteristic peak of SiC near 800 $cm^{-1}$. b) Evolution of XPS spectra of ECR-CVD nanographene with time. The left dashed line indicates the position of SiC and the right dashed line marks the $sp^2$ C–C peak at 284.4 eV. The SiC peak appears in the beginning of growth, but is becoming indiscernible after 3 min of growth due to the emerging nanographene which gives rise to an intense $sp^2$ C–C peak.

In **Figure 4**a we compare the Raman spectra of nanographene grown on copper and on quartz. Three prominent features appear at 1350 (D peak), 1590 (G peak), and 2700 $cm^{-1}$ (2D peak) in both spectra. The G peak is caused by the first order Raman scattering process; it is characteristic of $sp^2$ hybridization and involves the in-plane optical phonon $E_{2g}$ near the Γ point of the phonon band structure. For the growth on quartz, the G peak is merged with a D′ peak due to defects in the film. Subtracting the D′ mode contribution, a sharp *G* peak profile is expected that is distinct from that of amorphous carbon and diamond-like films grown by a similar method,[20–22] indicative of a well-graphitized film on the oxide. In a further comparison with graphite, the G peak exhibits a remarkable blueshift (from 1582 to 1590 $cm^{-1}$), which can be partly due to the nanocrystalline nature of the film,[23] partly doping[24] and partly to the substrate effects (strain).[25] To differentiate the two substrate

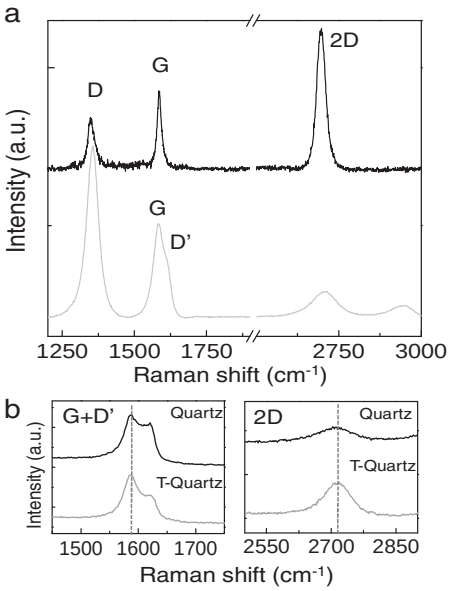


**Figure 4.** a) Raman spectra of ECR-CVD graphene grown on copper (upper) and of ECR-CVD nanographene grown on quartz. The spectra were taken by 488 nm laser excitation. b) Comparison of the G and 2D peaks of nanographene before (quartz) and after (T-quartz) transfer from a quartz to a silicon substrate. The 2D peak increases by a factor of 2.5 after the transfer.

effects, we transferred the nanographene film to another silicon substrate and compare the Raman spectra before and after the transfer (Figure 4b). It was found that the G and 2D peak positions are almost unchanged after the transfer, excluding the substrate-induced strain as the primary cause.[26] However, a doping effect (or more precisely the SiC-induced doping) should not be rule out at this time. The SiC buffer layer can induce electrons in nanographene, resembling the N-type doping in epitaxial graphene grown on SiC,[27–29] and results in a suppressed 2D peak. After transfer, the 2D intensity can be increased by a factor of 2–3, with intensity ratio $I_{2D}/I_G \approx 0.5$–1 (Figure 4b). This picture is also supported by the transport measurements in which only unipolar hole transport is seen in the wide range of gate sweeps due to the strong N-type doping on nanographene films.

The D peaks in Figure 4a reflect a common feature of defect density in the graphene grown using plasma. For the growth on quartz, large numbers of domain boundaries also account for the strong D peak in the spectrum, in accord with the TEM images which show that the polycrystalline nanodomains make up the primary structure in oxide-catalyzed nanographene films. The domain size $L_a$ can be estimated by the formula: $I_D/I_G = C(\lambda)/L_a$, where $I_D/I_G$ stands for the D over G peak intensity ratio and $C(\lambda) \approx 4.4$ nm for excitation at $\lambda = 488$ nm.[30,31] This yields an average domain size of 2–3 nm, close to that measured by TEM.

Transport measurements of nanographene show temperature-sensitive conductance changes (**Figure 5**a). Below 100 K, a more pronounced conductivity drop is produced, resembling the reduced graphene oxide and hydrogenated graphene in which nanoscaled clusters form.[32–34] The best linear fits of the temperature-dependent data were obtained by plotting $\ln(I/A)$ versus $T^{1/3}$, implying variable range hopping as a plausible charge-transport mechanism in nanographene. Variable range hopping involves consecutive inelastic tunneling processes between two localized states and has been frequently observed in disordered systems. This phenomenon is consistent with the fact that our nanographene films are composed of intact honeycomb nanostructures embedded in a defective carbon matrix. Transport in the field-effect transistor configuration shows that the pristine nanographene is N-type (Figure 5b), further confirming the presence of SiC. The charge neutrality point is not found within the back gate voltage sweeps in all measured conductance vs. gate voltage curves ($G_{ds}$–$V_{gs}$) curves. After transfer of the nanographene to another silicon substrate, the charge neutrality point appears close to the zero gate voltage in the

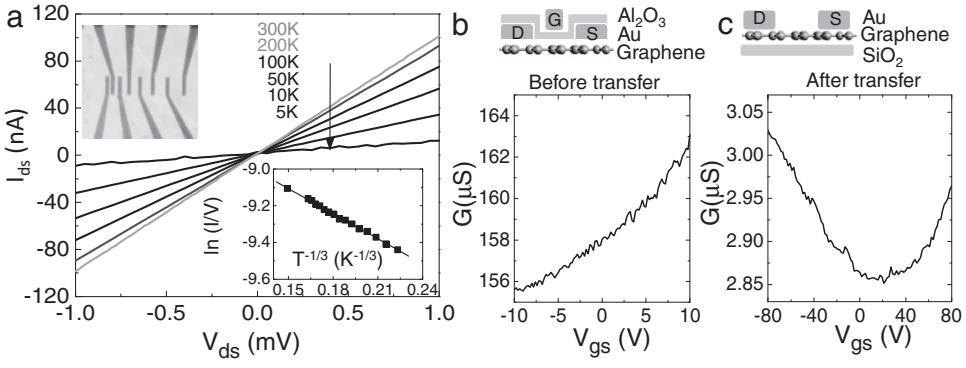


**Figure 5.** Characterizations of electrical properties of ECR-CVD nanographene grown on quartz. a) Output characteristics of field-effect transistors at different temperatures. The upper-left inset shows the optical image of the device. The lower-right inset is the plot of $\ln(I/A)$ versus $T^{-1/3}$ at low bias (10 mV). The good linear fit indicates the presence of charge transport barriers for two-dimensional variable range-hopping conduction. b) Transfer characteristics of top-gated field-effect transistors at room temperature. The devices were fabricated directly on pristine graphene grown on quartz. The gate dielectric was made of 60 nm thick $Al_2O_3$ by atomic layer deposition. The devices show electron conduction at $V_{gs} = 0$. c) Transfer characteristics of back-gated field-effect transistors at room temperature. The nanographene film was transferred to a new Si substrate with 300 nm oxide. The devices show both electron and hole conductions within the voltage of gate sweeps.

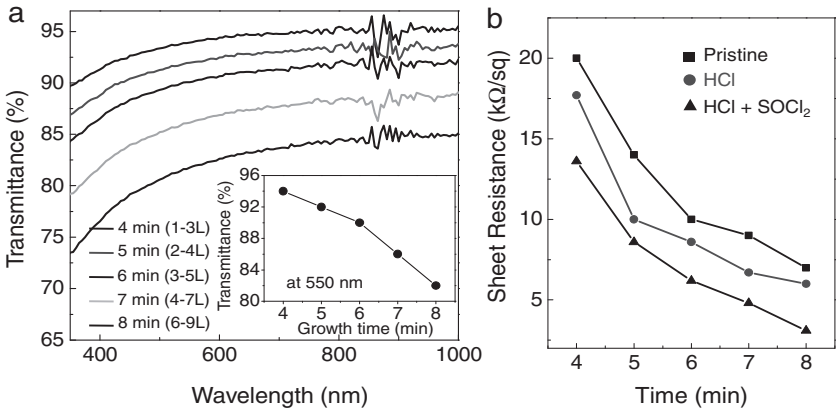


**Figure 6.** a) Optical transmittance of ECR-CVD nanographene grown on quartz, with different film thickness. The inset compares the transmittance at 550 nm for different growth durations. b) The sheet resistance decreases as the film thickness increases; it also decreases with increasing doping by chemical functionalization in HCl and $SOCl_2$ aqueous solutions.

back gate measurements (Figure 5c). It should be noted that although $Al_2O_3$ gate dielectrics may also cause week doping and shift the charge neutrality point accordingly, a substantial shift to a negative gate voltage as shown in Figure 5b is not expected due to the large gate capacitance of the $Al_2O_3$ film.

The optical transparency and sheet resistance of nanographene films grown on glass was also investigated. **Figure 6**a shows the transmittance of samples grown at different durations, with nanographene layers estimated by light transmittance in combination with TEM. The light transmittance decreases almost linearly as growth time increases. The thinnest pristine nanographene films exhibit transmittance of 94% at a wavelength of 550 nm and a sheet resistance of approximately 20 kΩ $sq^{-1}$, an order of magnitude higher than that of typical CVD graphene grown on metals, but still 1–2 orders of magnitude lower than that of well-reduced graphene oxide without doping.[35] The sheet resistance drops and gradually saturates as growth time increases. Acid treatment in HCl aqueous solution and functionalization in $SOCl_2$ are found to be of help in the reduction of the sheet resistance (Figure 6b). **Figure 7** compares our work with other reported studies. Despite the fact that the best sheet resistance of our nanographene film is not comparable with other CVD graphene grown at 1000 °C,[36,37] the ECR-CVD growth method provides a greener (lower temperature) and direct deposition of nanographene layers on insulating substrates. After simple doping, the sheet resistivity of our nanographene films is still better than those obtained by chemical exfoliation,[32,38,39] graphene grown on Cu at low temperature,[40] and nanographene sinthetized at higher temperatures.[41] Using a more effective molecule such as bis(trifluoromethanesulfonyl)imide[42] for doping, the sheet resistivity of the grown films is anticipated to be further decreased.

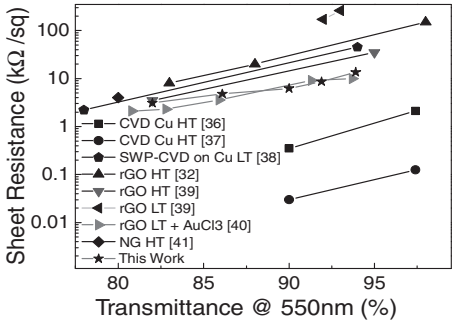


**Figure 7.** Comparison of resistivity and transmittance for different graphene films reported. HT stands for high temperature process (around 1000 °C) and LT for low temperature process (less than 500 °C).

## 3. Conclusions

We show that direct deposition of nanographene on silicon oxides, a process free of metal catalysts, can be achieved using an ECR-CVD method. Wet etching and transfer are thus unnecessary, leaving the nanographene films free from residual metal impurities or polymer contamination. Studies by transmission electron microscopy reveal that hexagonal carbon networks form nanodomains in a continuous film. Spectroscopic analysis shows that a SiC layer appears at the interface between nanographene film and $SiO_2$, highlighting the importance of carbide in the growth of graphene using oxides as catalysts. The proposed method may boost graphene applications in fields such as sensors, transparent conductive electrodes, electromagnetic interference shielding, electrical interconnects, and other electronic devices.

## 4. Experimental Section

*Graphene Deposition*: Commercially available pure $SiO_2$ dry oxide, quartz, and glass were used in the ECR-CVD growth of nanographene. All the oxide substrates used in the growth process were first cleaned by sonication in acetone, isopropyl alcohol, and de-ionized water. After cleaning, the substrate was place in the ECR-CVD chamber. When the vacuum reached $1 \times 10^{-6}$ Torr, Ar flow was introduced at a rate of 5 sccm and the plasma was ignited at a partial pressure of $6 \times 10^{-3}$ Torr at 400 W for 5 min, thus removing organic residues from the substrate surface. The temperature was then raised to above 400 °C under high vacuum. When the temperature stabilized, argon and ethylene flows were opened (Ar: 0.12 sccm; $C_2H_4$: 0.12 sccm) and the plasma was ignited with powers starting from 800 to 1600 W depending on the growing temperature. The growth rate is material dependent, and the typical growth time for a thin continuous nanographene film on $SiO_2$ is about 4 min. Following the growth, the plasma was turned off, and pure hydrogen flow was introduced for 10 min annealing at the same temperature. Finally, the sample was cooled down to room temperature under high vacuum.

*TEM Measurements*: TEM observations were conducted for ECR-CVD nanographene sheets grown on quartz and $SiO_2$. The substrate was first covered with a thin layer of poly(methyl methacrylate) (PMMA), followed by wet etching in a BOE solution for few hours. The PMMA, along with the attached nanographene film, was transferred onto a Mo grid (Quantifoil). The PMMA was then removed with acetone, followed with $CO_2$ critical point drying, followed by 1 h annealing in a hydrogen atmosphere at 250 °C. Electron microscopy characterizations were conducted using a JEOL 2100F transmission electron microscope equipped with a cold field emission gun and two DELTA correctors. Acceleration voltage of 60 kV was used throughout the measurements with specimens at ambient temperature. The TEM images were recorded by a Gatan CCD (model 894) with a typical exposure time of 1 s. For

STEM imaging, we used a 0.1 nm probe with current of 15 pA. For spectroscopy, we used a Gatan-Gif Quantum system, specially designed for low acceleration voltage operations.

*Raman and Transmittance Measurements*: A high-resolution Micro Raman Spectrometer (LabRaman 800, Horiba Jobin Yvon) equipped with a 100× objective was used to provide a diffraction-limited spot size of approximately 1 μm. Laser excitation was either $\lambda = 488$ nm or $\lambda = 514$ nm, and the power level was set at approximately 1 mW to avoid heating or damage to the sample. To compare the Raman spectra of nanographene grown on different oxides, the integration time was set at 20 s over all points on all substrates. For transmittance measurements, we used a LAMBDA 750 UV/Vis/NIR spectrophotometer (Pekin-Elmer). Sheet resistance was measured using the four-probe method in a Loresta-EP MCP-T360 low resistance meter (Mitsubishi). Prior to the sheet resistance measurements, the four-probe tips were cleaned using ethanol and air dried

*Transport Measurements*: The ECR-CVD nanographene grown on quartz was used for electrical measurements in the configuration of field-effect transistors. PMMA in a two-layer structure (950 and 230 K) was spin-coated on the grown nanographene film, followed by baking at 160 °C for 1 h. Electron beam lithography was carried out using a JSM 840A scanning electron microscope equipped with an Elphy Quantum e-beam writer (Raith). The exposed PMMA was then developed with methyl isobutyl keton (MIBK) and isopropyl alcohol in a ratio of 1:3. Gold contacts with a thin Cr adhesion layer (2 nm) were evaporated after the development. Atomic layer deposition (ALD-Savanah, Cambridge Nanotech) was used to deposit an $Al_2O_3$ layer (60 nm) as the top-gate dielectrics. Keithley 2400 and 2000 were respectively used as a current/voltage source and multimeter for current–voltage measurements.

## Supporting Information

Supporting Information is available from the Wiley Online Library or from the author.

## Acknowledgements

The authors appreciate the support of JST-CREST and Grant-in-Aid for Scientific Research from MEXT (#19054017), along with support from the NTHU booster project and Taiwan National Science Council under contract No. NSC 100-2112-M-007-014-MY3.

Received: October 8, 2011
Revised: December 9, 2011
Published online: February 17, 2012

[1] K. S. Novoselov, A. K. Geim, S. V. Morozov, D. Jiang, M. I. Katsnelson, I. V. Grigorieva, S. V. Dubonos, *Nature* **2005**, *438*, 197.
[2] C. Berger, S. Zhimin, X. Li, X. Wu, N. Brown, C. Naud, D. Mayou, T. Li, J. Hass, A. N. Marchenkov, E. H. Conrad, P. N. First, W. A. de Heer, *Science* **2006**, *312*, 1191.
[3] R. R. Nair, P. Blake, A. N. Grigorenko, K. S. Novoselov, T. J. Booth, T. Stauber, N. M. R. Peres, A. K. Geim, *Science* **2008**, *320*, 1308.
[4] K. S. Kim, Y. Zhao, H. Jang, S. Y. Lee, J. M. Kim, K. S. Kim, J.-H Ahn, P. Kim, J.-Y Choi, B. H. Hong, *Nature* **2009**, *457*, 706.
[5] A. Reina, X. Jia, J. Ho, D. Nezich, H. Son, V. Bulovic, M. S. Dresselhaus, J. Kong, *Nano Lett.* **2009**, *9*, 30.
[6] R. S. Weatherup, B. C. Bayer, R. Blume, C. Ducati, C. Baehtz, R. Schlögl, S. Hofmann, *Nano Lett.* **2011**, *11*, 4154.
[7] D. Takagi, H. Hibino, S. Suzuki, Y. Kobayashi, Y. Homma, *Nano Lett.* **2007**, *7*, 2272.
[8] B. Liu, W. Ren, L. Gao, S. Li, S. Pei, C. Liu, C. Jiang, H.-M Cheng, *J. Am. Chem. Soc.* **2009**, *131*, 2082.
[9] A. Bachmatiuk, F. Borrnert, M. Grobosch, F. Schaffel, U. Wolff, A. Scott, M. Zaka, J. H. Warner, R. Klingeler, M. Knupfer, B. Buchner, M. H. Rummeli, *ACS Nano* **2009**, *3*, 4098.
[10] M. H. Rümmeli, A. Bachmatiuk, A. Scott, F. Börrnert, J. H. Warner, V. Hoffman, J. H. Lin, G. Cuniberti, B. Büchner, *ACS Nano* **2010**, *7*, 4206.
[11] J. J. Wang, M. Y. Zhu, R.A. Outlaw, X. Zhao, D. M. Manos, B. C. Holloway, *Appl. Phys. Lett.* **2004**, *85*, 1265.
[12] L. Zhang, Z. Shi, Y. Wang, R. Yang, D. Shi, G. Zhang, *Nano Res.* **2011**, *4*, 315.
[13] J. Sun, N. Lindvall, M. T. Cole, K. B. K. Teo, A. Yurgens, *Appl. Phys. Lett.* **2011**, *98*, 252107.
[14] S. K. Jerng, D. S. Yu, Y. S. Kim, J. Ryou, S. Hong, C. Kim, S. Yoon, D. K. Efetov, P. Kim, S. H. Chun, *J. Phys. Chem. C* **2011**, *115*, 4491.
[15] Y. C. Lin, C. Jin, J. C. Lee, S. F. Jen, K. Suenaga, P. W. Chiu, *ACS Nano* **2011**, *5*, 2362.
[16] T. Sasaki, H. Sawada, F. Hosokawa, Y Kohno, T. Tomita, T. Kaneyama, Y. Kondo, K. Kimoto, Y. Sato, K. Suenaga, *J. Electron Microsc.* **2010**, *59*, S7.
[17] P. W. Sutter, J. I. Flege, E. A. Sutter, *Nat. Mater.* **2008**, *7*, 406.
[18] A. Malesevic, R. Vitchev, K. Schouteden, A. Volodin, L. Zhang, G. van Tendeloo, A. Vanhulsel, C. van Haesendonck, *Nanotechnology* **2008**, *19*, 305604.
[19] A. J. Page, K. R. S. Chandrakumar, S. Irle, K. Morokuma, *J. Am. Chem. Soc.* **2011**, *133*, 621.
[20] K. Baba, R. Hatada, *Surf. Coat. Technol.* **1998**, *103*, 235.
[21] S. F. Yoon, H. Yang, A. Ahn, Q. Zhang, *Diamond Relat. Mater.* **1998**, *7*, 70.
[22] K. Y. Li, Z. F. Zhou, C. Y. Chan, I. Bello, C. S. Lee, S. T. Lee, *Diamond Relat. Mater.* **2001**, *10*, 1855.
[23] A. C. Ferrari, J. Robertson, *Philos. Trans. R. Soc. London, Ser. A* **2004**, *362*, 2477.
[24] H. Medina, Y. C. Lin, D. Obergfell, P. W. Chiu *Adv. Funct. Mater.* **2011**, *21*, 2687.
[25] Z. Cheng, Q. Zhou, C. Wang, Q. Li, C. Wang, Y. Fang, *Nano Lett.* **2011**, *11*, 767.
[26] N. Ferralis, R. Maboudian, C. Carraro, *Phys. Rev. Lett.* **2008**, *101*, 156801.
[27] Z. H. Ni, W. Chen, X. F. Fan, J. L. Kuo, T. Yu, A. T. S. Wee, Z. X. Shen, *Phys. Rev. B* **2008**, *77*, 775416.
[28] C. Casiraghi, *Phys. Rev. B* **2009**, *80*, 233407.
[29] C. Faugeras, A. Nerriere, M. Potemski, A. Mahmood, E. Dujardin, C. Berger, W. A. de Heer, *Appl. Phys. Lett.* **2008**, *92*, 011914.
[30] F. Tuinstra, J. L. Koening, *J. Chem. Phys.* **1970**, *53*, 1126.
[31] D. S. Knight, W. B. White, *J. Mater. Res.* **1989**, *4*, 385.
[32] X. Li, G. Zhang, X. Bai, X. Sun, X. Wang, E. Wang, H. Dai, *Nat. Nanotechnol.* **2008**, *3*, 538.
[33] D. C. Elias, R. R. Nair, T. M. G. Mohiuddin, S. V. Morozov, P. Blake, M. P. Halsall, A. C. Ferrari, D. W. Boukhvalov, M. I. Katsnelson, A. K. Geim, K. S. Novoselov, *Science* **2009**, *323*, 610.
[34] G. Eda, C. Mattevi, H. Yamaguchi, H. K. Kim, M. Chhowalla, *J. Phys. Chem. C* **2009**, *113*, 15768.
[35] G. Eda, M. Chhowalla, *Adv. Mater.* **2010**, *22*, 2392.
[36] X. Li, Y. Zhu, W. Cai, M. Borysiak, B. Han, D Chen, R. D. Piner, L. Colombo, R. S. Ruoff, *Nano Lett.* **2009**, *9*, 4359.
[37] S. Bae, H. Kim, Y. Lee, X. Xu, J. S. Park, Y. Zheng, J. Balakrishnan, T. Lei, H. R. Kim, Y. I. Song, Y. J. Kim, K. S. Kim, B. Ozyilmaz, J. H. Ahn, B. H. Hong, S. Iijima, *Nat. Nanotechnol.* **2010**, *5*, 574.
[38] H. A. Becerril, J. Mao, Z. Liu, R. M. Stoltenberg, Z. Bao, Y. Chen, *ACS Nano* **2008**, *2*, 463.
[39] H. J. Shin, K. K. Kim, A. Benayad, S. M. Yoon, H. K. Park, I. S. Jung, M. H. Jin, H. K. Jeong, J. M. Kim, J. Y. Choi, Y. H. Lee, *Adv. Funct. Mater.* **2009**, *19*, 1987.
[40] J. Kim, M. Ishihara, Y. Koga, K. Tsugawa, M. Hasegawa, S. Iijima, *Appl. Phys. Lett.* **2011**, *98*, 091502.
[41] K. B. Kim, C. M. Lee, J. Choi, *J. Phys. Chem. C* **2011**, *115*, 14488.
[42] S. M. Kim, Y. W. Jo, K. K. Kim, D. L. Duong, H.-J. Shin, J. H. Han, J.-Y Choi, J. Kong, Y. H. Lee, *ACS Nano* **2010**, *4*, 6998.